Geomechanics and Engineering, *Vol. 27, No. 1 (2021) 87-99*
https://doi.org/10.12989/gae.2021.27.1.087

Compressive strength of flawed cylindrical specimens subjected to axial loading

Javad Karimi[1], Mostafa Asadizadeh*[2,3], Mohammad Farouq Hossaini[4], Samuel Nowak[3] and Taghi Sherizadeh[3]

[1]*School of Mining Engineering, College of Engineering, University of Tehran, 1439957131 Tehran, Iran*
[2]*Department of Mining Engineering, Hamedan University of Technology, Mardom Street, Hamedan, 65155 -579, Iran*
[3]*Department of Mining and Nuclear Engineering, Missouri University of Science and Technology, Rolla, MO 65409, U.S.A.*
[4]*School of Minerals and Energy Resources Engineering, University of New South Wales, Sydney, Australia*

(Received April 16, 2019, Revised May 25, 2021, Accepted October 1, 2021)

Abstract. Discontinuities are known to have a significant impact on the engineering characteristics of the rock masses, governing their potential failure pattern, increasing their deformation, and reducing their strength. In particular, the impact of non-persistent joints on the strength and failure mechanism of rock mass needs to be investigated further. The impact of different flaw geometrical characteristics such as flaw inclination, flaw length, flaw aperture, and flaw filling on uniaxial compressive strength of specimens has not been investigated thoroughly. In this paper, a series of uniaxial compression tests were conducted on cylindrical specimens containing an open central flaw. The effect of different parameters such as flaw inclination, flaw length, flaw aperture, and filling on the uniaxial compressive strength of specimens have been investigated through laboratory experiments. Response Surface Methodology (RSM) is adopted to analyze the impact of flaw parameters on the compressive strength of the constructed samples. The results of the experiments show that flaw inclination and flaw length have a significant impact on the peak strength of the samples, meaning that strength increases by growing of flaw angle and decreases by increasing of flaw length. In addition, at a low flaw length, aperture affects the UCS significantly, while by increasing flaw length, its effect decreases dramatically, and strength drops at a flaw inclination of 45 degrees. Conversely, at a higher flaw length, by increasing flaw inclination, the UCS increases constantly. It also has been observed that changing the flaw aperture had no important effect on the peak strength.

Keywords: filling material; open flaw; RSM; strength anisotropy; UCS

1. Introduction

As an engineering material, rock mass can exhibit complex behaviors. In small scale, intact rock can behave as a continuous and isotropic media, but in large scale, its continuity is affected by discontinuities which cause the rock mass to behave as an anisotropic and heterogeneous material. Discontinuities include shear and weakness planes, joints, cracks, fissures and faults which control the mechanical behavior of rock mass. In any rock engineering practice, an accurate measure of the axial strength of the material is of paramount importance for designing a stable and safe structure. In both surface and underground rock engineering projects, experiments should be conducted to estimate the uniaxial compressive strength in different rock units found at the site. The axial loading of rock structures with non-persistent joints is especially common in coal pillars, and the sidewalls of underground openings (Brady and Brown 2008). Many experimental investigations have been carried out on pre-cracked specimens, the results of which have indicated that the geometry characteristics of flaws have a key effect on the mechanical behavior of fractured rock (Nemat-Nasser and Horii 1982, Bobet and Einstein 1998, Wong and Chau 1998, Yang *et al.* 2008, 2009, Park and Bobet 2009, Lee and Jeon 2011, Liu *et al.* 2015, Asadizadeh, Moosavi and Hossaini 2018, Yin *et al.* 2018, Asadizadeh *et al.* 2019). Despite the importance of studying the strength behavior of anisotropic rocks, the experimental investigation of these types of rocks have encountered some issues. Most studies are associated with providing uniform and duplicated natural specimens mainly due to weathering, different texture, crack property, coring angle and etc. Moreover, creating a flaw in natural specimens requires advanced tools which are time consuming and expensive to use. One of the solutions to solve this problem is fabricating synthetic specimens (Bobet and Einstein 1998, Bobet 2000, Sagong and Bobet 2002, Park and Bobet, 2009 Mostafa Asadizadeh *et al.* 2016, Asadizadeh *et al.* 2018, Asadizadeh *et al.* 2019). These synthetic specimens are more uniform and similar in comparison to natural ones. For this purpose, many investigations have been conducted using synthetic specimens, which can be cast in a short time and numerous number with a specific shape at very low cost (Nemat-Nasser and Horii, 1982, Bobet 2000, Li *et al.* 2005, Yang and Jing 2011, Chen *et al.* 2012, Huang *et al.* 2016, Asadizadeh *et al.* 2018, Gemi *et al.* 2018, Han *et al.* 2018,

*Corresponding author, Ph.D.
E-mail: m.asadizadeh@hut.ac.ir, ma84g@mst.edu

ISSN: 2005-307X (Print), 2092-6219 (Online)

Asadizadeh and Rezaei 2019, Özbek and Bozkurt 2019, Özbek *et al.* 2019, Özbek *et al.* 2020, Özkılıç *et al.* 2021, Özbek, 2021).The mechanical behavior of artificial blocks containing two flaws was investigated and the results showed flaw length is one of the important factors governing the failure mechanism of specimens (Nemat-Nasser and Horii, 1982). A group of uniaxial and biaxial tests was performed on rectangular artificial specimens made of cement to study the mechanical response of clean jointed specimens under the effect of varying joint angle (Han *et al.* 2018). The cracking process of a single flaw is characterized by (Bobet, 2000), and they introduced wing and shear cracks. Wing cracks are known as tensile failure features which usually initiate at the tips of cracks and develop in the direction of the major compressive stress in a stable manner. Secondary cracks also develop from the tips of the cracks; however, they form later on during the loading progression, and propagate steadily, often times in a coplanar manner with respect to the initial flaw. An extensive experimental study on crack development of joints under axial loading was conducted by (Li, Chen and Wang, 2005). They also reported the initiation and propagation of two types of cracks form the crack tips (i.e., wing cracks and secondary cracks). Another research conducted by (Yang and Jing, 2011) aimed at investigating the mechanical properties of fissured cylindrical specimens under different flaw angles. The specimens were cast with a mixture of cement, quartz and water and the results indicated that the UCS and Young's modulus of a pre-cracked sample decreases for the lower level of fissure angle (45°) and increases with increasing fissure angle (up to 75°). Crack initiation from tips of single fissure in brittle sandstone under uniaxial loading was studied by (Huang *et al.* 2016). They introduced nine different crack types by analyzing the final failure mode of flawed sandstone. Results revealed that with the increase of the joint angle UCS formed an asymmetrical “V” shape and its minimum value occurred at joint angle 15˚. The effect of flaw angle and rock bridge angle on strength and deformational characteristics of cubic gypsum specimens with double parallel pre-fabricated flaws under UCS test was studied by (Liu *et al.* 2015). The effect of flaw angle and bridge angle were investigated, and the results revealed that strength and deformation behavior of flawed samples are affected by variation of flaw and bridge angle. An extensive experiments on tabular-shaped rock-like blocks having two preexisting parallel rough non-persistent joints subjected to the uniaxial compressive load were carried out by means of physical modeling (Asadizadeh *et al.* 2018, Asadizadeh and Rezaei 2019), and the effect of four parameters mainly including joint bridge length, bridge angle, roughness coefficient, and joint inclination on mechanical behavior was investigated. The results of RSM analysis revealed that the interaction effect of the joint parameters had a remarkable impact on the compressive strength and deformation modulus.

A comprehensive study associated with the effect of flaw geometries in a cylindrical specimen under uniaxial compression strength has not been performed yet, therefore in this paper, the effect of flaw inclination, flaw length, flaw aperture, the flaw filling and their interaction on strength behavior of cylindrical specimens have been studied thoroughly. A large number of artificial, flawed specimens with different flaw geometry were cast, and the interaction effect of flaw parameters on compressive strength was investigated using historical design response surface methodology. Furthermore, the effect of filled flaw on strength behavior is studied and a comprehensive comparison between unfilled and filled flaws has been carried out.

2. Sample preparation and laboratory testing

2.1 Sample preparation

The synthetic samples were made of a mixture of Dental Plaster and water. First, water and plaster were mixed in a blender with a ratio of 0.45 by weight. Then the mortar was placed in a cylindrical plastic mold with internal dimensions of 54 mm and 122 mm height. The mold was made of a Polyethylene tube with a lateral all-over crack which facilitates the removal of specimen from mold after its preparation. The crack was fasten using a clamp, and the pre-existing flaw in the specimen was created by inserting a single Plexiglass blade with different dimensions (Fig.1) into the slot and through the mortar, resulting in a flaw length (2a) of 13 mm, 26 mm, and 39 mm and aperture of 1.2 mm, 2 mm, and 2.8 mm.

The location and orientation of slot were varied to provide different flaw inclination and length (see Fig.2), and the joint inclination was set to 0˚,15˚, 30˚, 45˚,60˚, and 75˚. The mold with wet plaster was vibrated for 1 min using a vibrating table and after 4 minutes the Plexiglass was removed from the sample, which was then removed from the mold and placed in a room at a temperature 20˚C for 14 days. After curing, both ends of the sample were cut and machined to ensure flat contact surfaces. Since the samples were fabricated with high precision and accuracy, one sample was prepared for each test.

2.2 Sample testing

To study the strength of specimens, the maximum axial stress was recorded as UCS for all flawed samples, and the stress-strain curve for five intact-samples was recorded. The UCS experiments on intact cylindrical samples were conducted according to (ASTM-D7012-14, 2014), and axial stress and strain, as well as lateral strain, were recorded, so UCS and elastic modulus, as well as Poisson's ratio (ASTM-E 132-97, 1997), were estimated. Moreover, five Brazilian discs with a diameter of 54 mm and thickness of 27 mm were subjected to diametric loading according to ISRM suggested method (Bieniawski and Hawkes, 1978) to obtain the indirect tensile strength of the artificial material. Mechanical and physical characteristics of synthetic material are presented in Table 1.

In this paper, 54 UCS experiments were carried out on the specimens utilizing a servo-hydraulic Rock Mechanics Testing System (MTS) with a maximum loading capacity of

Table 1 Mechanical and physical characteristics of artificial specimens

Physical or mechanics parameter	Value
Diameter/height	2.26
Water/plaster	0.45
Density (gr/cm^3)	1.20
Unconfined compressive strength (σ_c, MPa)	21.30
Elastic modulus (E, GPa)	7.00
Indirect tensile strength (σ_t, MPa)	3.70
Poisson's ratio (υ)	0.27

(a) (b)

Fig. 3 (a) Schematic view of specimen and flaw geometry parameters, 2a: flaw length, "A": flaw aperture and θ: flaw inclination and (b) Loading apparatus

Table 2 the flaw geometry characteristics and the results of uniaxial compressive tests

Sample NO.	θ (˚)	2a (mm)	A (mm)	UCS (MPa)	Sample NO.	θ (˚)	2a (mm)	A (mm)	UCS (MPa)	Sample NO.	θ (˚)	2a (mm)	A (mm)	UCS (MPa)
1	0	13	1.2	11.13	19	0	26	1.2	6.50	37	0	39	1.2	1.49
2	15	13	1.2	14.49	20	15	26	1.2	6.42	38	15	39	1.2	1.28
3	30	13	1.2	15.24	21	30	26	1.2	7.40	39	30	39	1.2	2.82
4	45	13	1.2	16.10	22	45	26	1.2	6.97	40	45	39	1.2	4.28
5	60	13	1.2	15.92	23	60	26	1.2	11.43	41	60	39	1.2	5.60
6	75	13	1.2	17.38	24	75	26	1.2	14.72	42	75	39	1.2	10.34
7	0	13	2.0	11.81	25	0	26	2.0	5.09	43	0	39	2.0	1.11
8	15	13	2.0	13.14	26	15	26	2.0	5.48	44	15	39	2.0	1.19
9	30	13	2.0	14.90	27	30	26	2.0	6.33	45	30	39	2.0	2.99
10	45	13	2.0	13.01	28	45	26	2.0	7.06	46	45	39	2.0	3.33
11	60	13	2.0	18.23	29	60	26	2.0	10.44	47	60	39	2.0	5.13
12	75	13	2.0	18.68	30	75	26	2.0	15.11	48	75	39	2.0	10.01
13	0	13	2.8	12.95	31	0	26	2.8	4.53	49	0	39	2.8	1.19
14	15	13	2.8	13.27	32	15	26	2.8	6.85	50	15	39	2.8	1.07
15	30	13	2.8	13.95	33	30	26	2.8	7.36	51	30	39	2.8	2.14
16	45	13	2.8	12.54	34	45	26	2.8	7.23	52	45	39	2.8	3.85
17	60	13	2.8	16.87	35	60	26	2.8	8.30	53	60	39	2.8	4.88
18	75	13	2.8	17.85	36	75	26	2.8	12.28	54	75	39	2.8	9.72

Fig. 4 Synthetic Flawed specimens with filled flaw and θ=45°

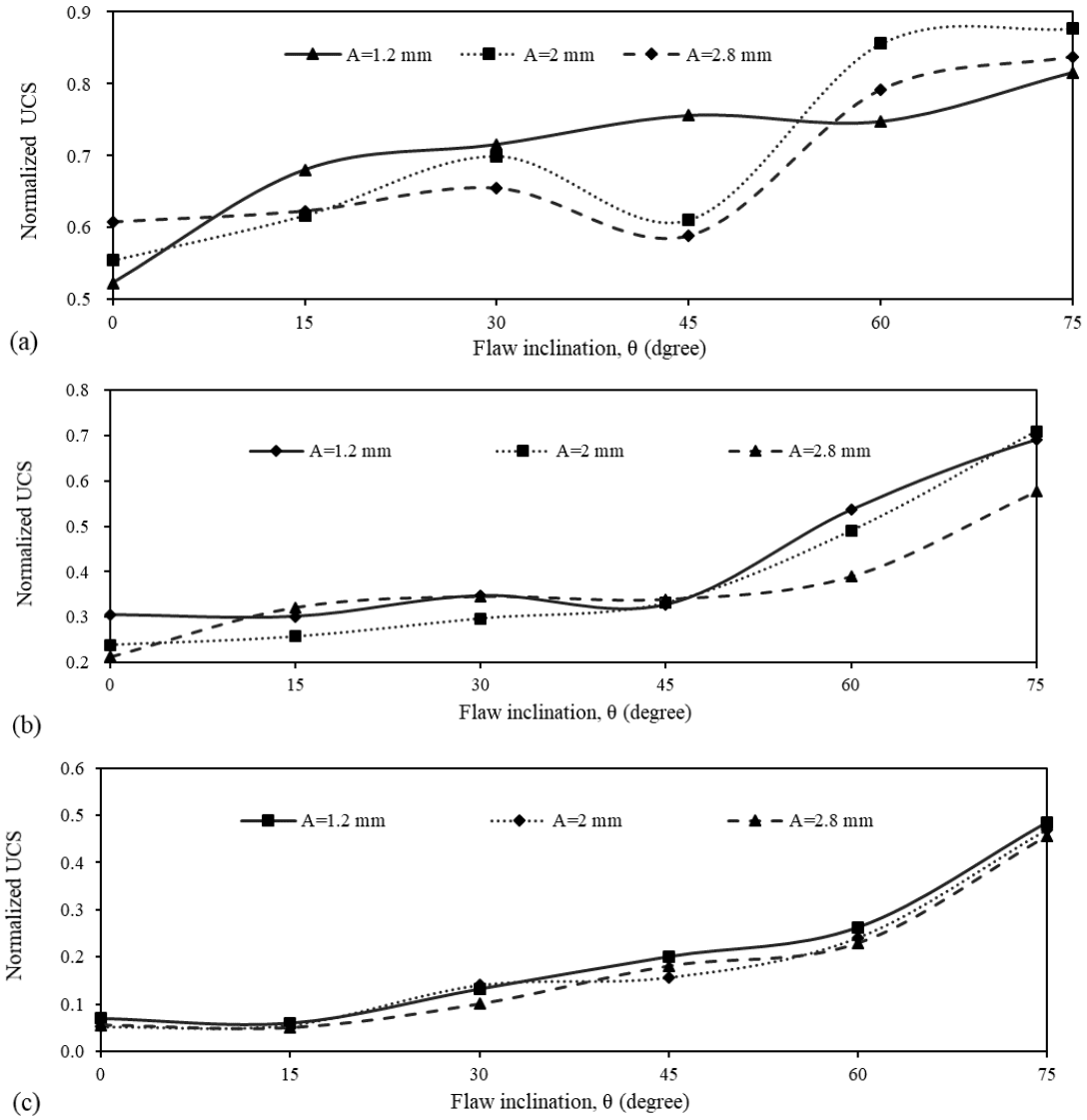

Fig. 5 The variation of UCS with respect to the flaw inclination (a) 2a=13 mm, (b) 2a=26 mm and (c) 2a=39 mm

400 ton. The axial strain rate was fixed at 0.005 mm/s according to (ASTM-D7012-14, 2014), to make the record of the crack development process more achievable. Fig. 3 illustrates the loading machine and flaw geometry parameters.

A digital camcorder was employed to monitor the crack development and record crack initiation and coalescence using a sampling rate of 20 fps (frames per second). The specimen was loaded until failure, or cracks had coalesced. The flaw geometry parameters are illustrated in Fig. 3(a),

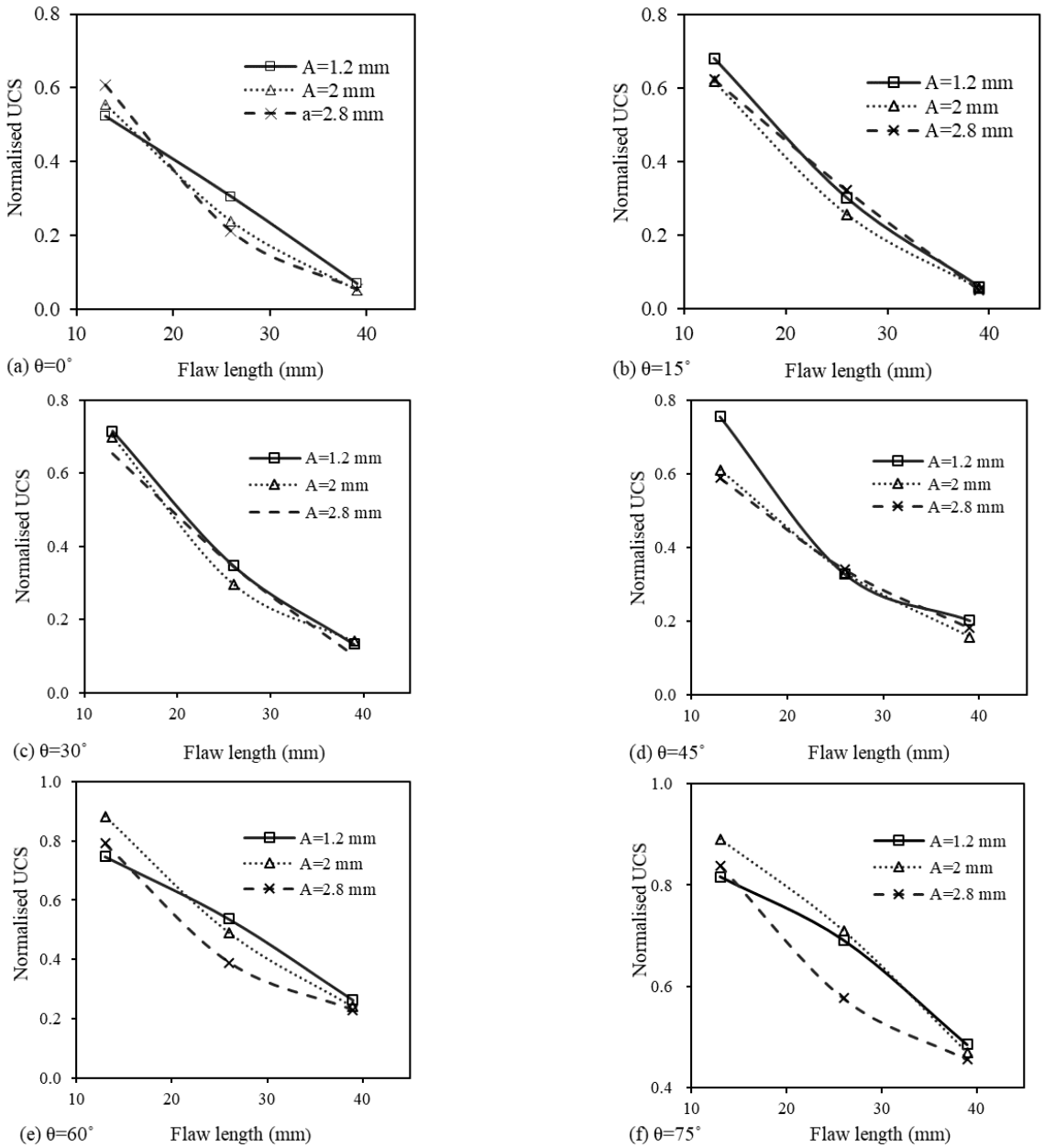

Fig. 6 Variation of UCS with respect to the flaw length and aperture

and it is noteworthy that aperture is defined for unfilled flaws. The characteristic of each specimen and the results of uniaxial strength are presented in Table 2.

In addition, the effect of the flaw filling on strength behavior was investigated by examination of 6 synthetic specimens filled by cement mortar. The filling was fabricated using Portland Cement Type II, with 45 MPa compressive strength. The flaw inclination varied from 0˚ to 75˚ in 15˚ intervals. The length and the width of the flaw were set to 26 mm and 2.8 mm, respectively. A view of specimen with filled flaw is shown in Fig. 4.

3. Experimental results

3.1 Effect of unfilled flaw inclination on UCS

In order to investigate the effect of unfilled flaw inclination on peak strength of specimens, a series of specimens were created according to Table 2. As it can be seen from this table, the peak strength of all flawed specimens is less than the intact one**.** The uniaxial compressive strength of the intact specimen was 21.3 MPa, while the peak strength of specimens containing a single, central flaw varied from 1.07 MPa (β= 15˚, 2a= 39 mm, A= 2.8 mm) to 18.68 MPa (β= 75˚, 2a= 13 mm, A= 2 mm). The strength reduction rate of flawed specimens is reported between 5% and 88%. The effect of flaw inclination on peak strength of cylindrical specimens is shown in Fig. 5, in which the flaw length varies from 13 mm to 26 mm and 39 mm. Fig. 5(a), 5(b), and 5(c) illustrates the relationship between flaw inclination, flaw aperture and the measured UCS for a constant flaw length of 13 mm, 26 mm, and 39 mm respectively.

As can be inferred from Figs. 5(a)-5(c), UCS has

Table 3 The temporal sequence of initiated cracks

Specimen Code	Primary cracks	Secondary cracks	Specimen Code	Primary cracks	Secondary cracks	Specimen Code	Primary cracks	Secondary cracks
1	T1/T1		19	T1/T1		37	T1/T1	
2	T1	ST2/T3	20	T1/T1		38	ST1/T1	
3	T1/T1		21	T1/T1	ST2	39	T1/T1	ST2
4	T1/ST1/S1		22	T1/T1		40	T1/T1	
5	T1/T1		23	T1/T1	ST2	41	T1/T1	ST2/S3
6	T1/S1		24	T1/T1		42	T1/T1	
7	T1/T1		25	T1/T1	ST2	43	T1/S1	
8	T1/T1		26	T1/T1	ST2/S3	44	T1/T1	
9	T1/T1	ST2	27	T1/T1	ST2/S3	45	T1/T1	
10	T1/T1		28	T1/T1		46	T1/T1	
11	T1/T1		29	T1/T1		47	T1/T1	
12	T1/T1/S1/S1		30	T1/ST1		48	T1/T1	
13	T1/T1		31	T1/T1		49	T1/T1	
14	T1/T1		32	T1/T1		50	T1/T1	
15	T1/T1		33	T1/T1		51	T1/T1	
16	T1	ST2/T3	34	T1/T1		52	T1/T1	
17	T1/T1	ST2	35	T1/T1		53	T1/T1	ST2
18	T1/T1		36	T1/T1		54	T1/T1	

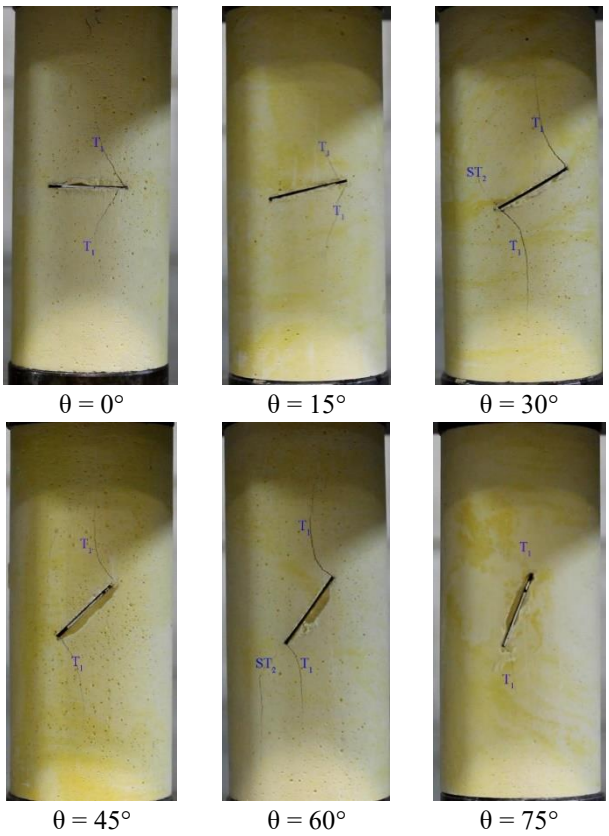

Fig. 7 The effect of flaw inclination on failure pattern of specimens in which A= 1.2 mm and 2a= 26 m—

increased with the increase of flaw inclination angle in all flaw's geometry. In all flawed specimens, minimum UCS has been obtained at the flaw angle of 0˚, except specimens with the flaw angle of 45˚ which have a length of 13 mm and the aperture of 2.8 mm (Fig. 5(a)). The maximum value of UCS has occurred at the flaw angle of 75˚ in all flaw geometries. Additionally, based on the plots (Fig. 5), the variation of flaw aperture does not affect UCS in samples with higher flaw length, but at low level of flaw length the sample with lower aperture exhibits a different mechanical behavior from the other samples.

3.2 Effect of unfilled flaw length and aperture on UCS

In order to have an in-depth understanding of the effect of flaw length and aperture on UCS, the results were presented in accordance with those two parameters (Fig. 6). To do so, the flaw length has taken as 13, 26 and 39 mm, and flaw aperture was 1.2 mm, 2 mm and 2.8 mm.

As it can be seen in Fig. 6, by increasing flaw length UCS decreases remarkably at all flaw inclinations, and flaw aperture has no significant effect on UCS. In addition, it indicates that the percentage of UCS reduction at different level of flaw inclination is different; in another words, by increasing flaw length at low level of flaw inclination (i.e., θ=0˚ and 15˚) UCS almost decreases by 60 %, and at its middle level (i.e., θ=30˚ and 45˚) it decreases nearly 76 % and, finally, at its highest level (i.e., θ=60˚ and 75˚), UCS reduces by 88 %. It can be indicated that the percentage of UCS reduction at deeper angles of flaw is much more than its reduction at lower angle, and flaw aperture does not contribute to this reduction.

3.3 Cracking process

The cracking process of specimens is discussed in this

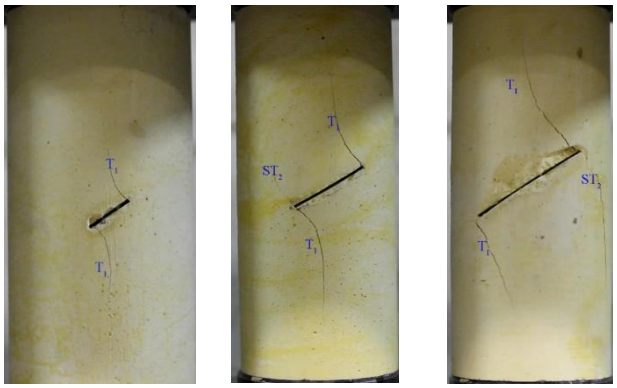

2a= 13 mm 2a= 26 mm 2a=39 mm

Fig. 8 The effect of flaw length on failure pattern of specimens in which A= 1.2 mm, θ = 30°

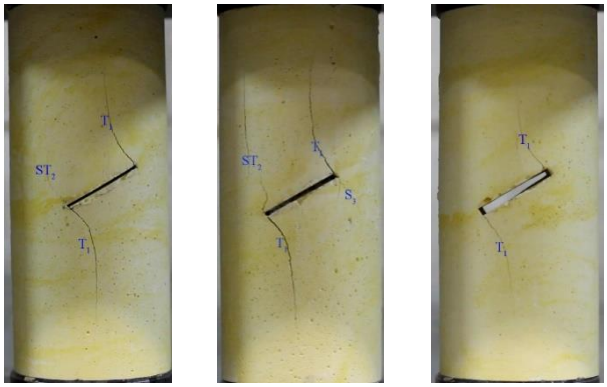

A= 1.2 mm A= 2 mm A= 2.8 mm

Fig. 9 The effect of flaw aperture on failure pattern of specimens in which L=26 mm, θ = 30°

section. As axial loading continues, a new series of cracks initiate from the surface of flaws. These newborn cracks include all three types of tensile cracks, shear cracks and mixed tensile-shear cracks classified by (Wong and Einstein, 2009).

3.3.1 Cracking pattern classification

The temporal sequence of initiated cracks has been presented in table 3. In the table, the T, S and ST letters indicate tensile cracks, shear cracks and mixed tensile-shear cracks, respectively. Moreover, numbers 1, 2 and 3 show the temporal sequence of initiated cracks, respectively. As an example, T1/T1 indicates two tensile cracks which have been initiated simultaneously as primary cracks or ST2 and S3 show mixed tensile shear crack and shear crack which have initiated after primary crack as secondary cracks. As it can be seen, tensile wing cracks are the first cracks which have been initiated at low value of loading (Table 3), followed by other types of cracks such as shear cracks and mixed tensile-shear cracks at higher level of loading. However, in a few specimens, other types of cracks (shear crack and mixed tensile-shear crack) have initiated with tensile cracks simultaneously as primary cracks.

3.3.2 The effect of flaw inclination on failure pattern

The effect of flaw inclination on crack development is shown in Fig. 7, in which flaw aperture and length are fixed

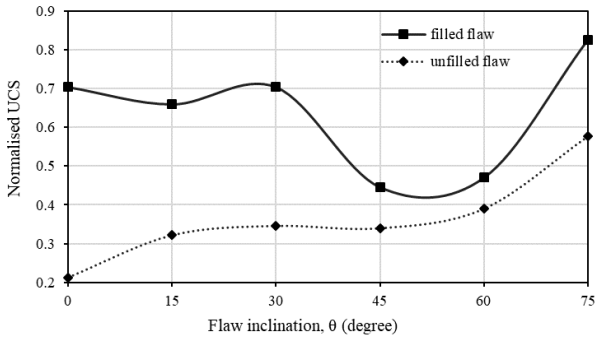

Fig. 10 The effect of filling of flaw on UCS

at A= 1.2 mm and L= 26 mm. From flaw angle 0° to 15°, joint type T1 initiates from right side of the flaws, and from θ = 30° to θ = 75° wing cracks T1 developed too. Crack ST2 formed in sample with θ = 60° at the left side of the flaw. The variation of UCS vs flaw angle for these specimens shows that the increase rate of UCS from flaw angle 0° to 45° is slow and after θ = 45°, UCS increases with a high increasing rate (see Fig. 5(b)).

3.3.3 The effect of flaw length on failure pattern

Flaw length can easily affect the UCS of specimens. The effect of flaw length at three levels of 13 mm, 26 mm and 39 mm are presented in Fig. 8, in which flaw aperture and angle are A= 1.2 mm, θ = 30°. In all three specimens, type T1 wing cracks develop at the crack tip, but at flaw length 26 mm and 39 mm cracks type ST2 developed as well. As presented in Fig. 6c, by increasing flaw length UCS decreases, and this may happen mainly because as flaw length increases, the flaw tips will be closer to the top and bottom of specimens, resulting in a lowered bearing capacity of the specimen.

3.3.4 The effect of flaw aperture on failure pattern

The effect of flaw aperture on failure pattern of specimens are presented in Fig. 9. The flaw aperture varied at three levels (i.e., 1.2 mm, 2 mm and 2.8 mm), and the failure pattern was recorded (see Fig. 9). In all models, crack type T1 initiates from flaw tip and develops toward loading boundaries. However, in specimens with A= 1.2 mm and A= 2 mm ST2 and S3 initiate from flaw tip respectively (see Fig. 9).

3.4 The Effect of flaw filling on UCS

In order to investigate the effect of filling material on UCS of flawed specimens, the flaw of 6 samples were filled with different joint inclination, and then subjected to axial loading. In this case, only the flaw inclination varied, and the flaw length and flaw aperture were constant at 26 mm and 2.8 mm, respectively. The flaw aperture was filled by a mortar of cement with water/cement ratio 1:1 and compressive strength 45 MPa which is much more than sample's strength. The effect of flaw inclination on UCS in both conditions with filled and unfilled flaw is presented in Fig.10.

Peak strength for specimens with filled flaw is more than the peak strength of specimens with unfilled flaw, and

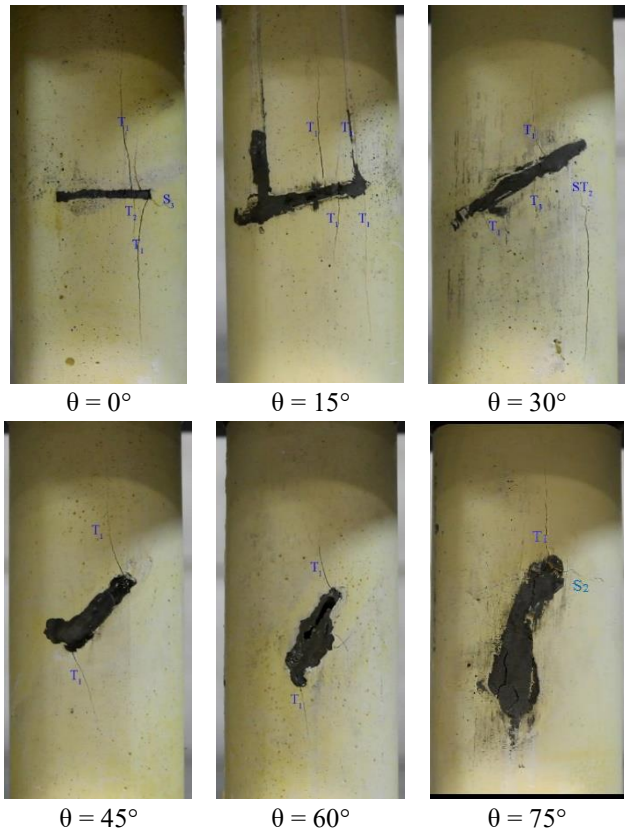

Fig. 11 The effec of flaw filling of UCS at different flaw angle (flaw apereture and length are keppt constant A= 2.8 mm and 2a= 26 mm)

for both of them it occurs at high level of flaw inclination (i.e., θ=75°). In the case of unfilled flaw, specimen with inclination angle of 0˚ has the minimum strength and specimen with the flaw inclination angle of 75˚ has the maximum strength. This may happen due to stress redistribution at the flaw tips which can trigger the growth of cracks before reaching the specimen to its peak strength. Although in the interval of flaw inclination from 15° to 45° UCS remains steady, increasing trend of UCS from θ=0˚ to θ=75˚is predominant. On the other hand, a typical "U" shape of strength anisotropy is occurred when the flaw is filled (see Fig. 10), and it drops to a minimum between θ=45°and θ=60°. This behavior reveals the capability of filling material to prevent crack initiation at low flaw angle. As for failure pattern of filled flaw specimens under axial loading, at low flaw angle specially θ = 15°, θ = 30° and high angle of θ = 75°, failure patter is completely different from unfilled specimens. It means that wing cracks barely initiated from crack tips and filling easily can transfer stress through the specimen. However, at angle θ = 45° and θ = 60° wing cracks initiate at crack tip and strength decreases (see Fig. 11).

4. Worked examples

4.1 RSM modeling

In order to study the impact of flaw geometry on UCS, the impact of θ, 2a and "A" on UCS were investigated statistically. Therefore, for further understanding Historical design of Response Surface Methodology (RSM) was adopted to investigate the mutual effects of the specimen properties on the response.

Table 4 Coded independent parameters and their corresponding levels for multiple regression modelling of UCS

Factor	Code	Level	
		-1	1
Flaw inclination (degree)	θ	0	75
Flaw length (mm)	2a	13	39
Flaw aperture (mm)	A	1.2	2.8

Table 5 Statistical parameter of RSM models

Statistical parameter	Model	Description
F-value	345,52	Model is significant
Adequate precision	61,459	Model can be used to navigate the design space
R2	0.9730	High correlation between the exponential and the predicted values
Adjusted-R2	0.9702	In a good agreement with their R^2 coefficient

4.2 Design of experiments and RSM

The design of experiments (DOE) methods, like RSM which are based on statistical and arithmetical approaches, have been developed to model a process and explain the interaction of factors on the response of a system (Montgomery 2001, Kirmizakis *et al.* 2014, Sodeifian *et al.* 2014, Yuan *et al.* 2015, Heidarzadeh *et al.* 2017, Asadizadeh *et al.* 2018a, b, Li *et al.* 2018). RSM is able to deal with a few number of experiments to investigate the interaction among variables and their impact on the response (Montgomery 2001). In this paper, a mathematical model was developed utilizing the Design-Expert 7 software and historical data design was employed to model RSM. The independent variables included in the modeling process are flaw inclination, flaw length and flaw aperture (Fig. 3a). The dependent variable is the peak strength, which can be expressed using a quadratic model as follows (Montgomery 2001, Kirmizakis *et al.* 2014, Heidarzadeh *et al.* 2018, Asadizadeh *et al.* 2018,).

$$y = \beta_0 + \sum_{i=1}^{3} \beta_i X_i + \sum_{i=1}^{3} \beta_{ii} X_i^2 + \sum_{i=1}^{3} \sum_{j=i+1}^{3} \beta_{ij} X_i X_j \quad (1)$$

where y is the response variable representing the UCS; β_{ii}, β_{ij}, β_i, and β_0 are regression coefficients; and X_i and X_j are the values of the independent variables coded in the program. The code and level of the independent variables are presented in Table 4.

4.3 Variance analysis (ANOVA)

The analysis of variance (ANOVA) technique was

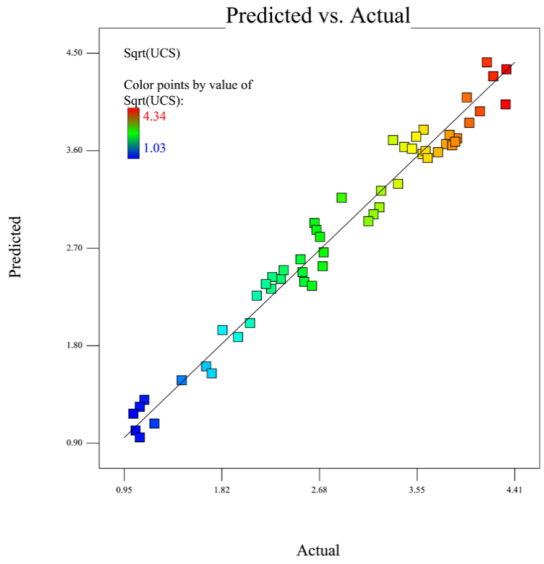

Fig. 12 The actual and predicted UCS models

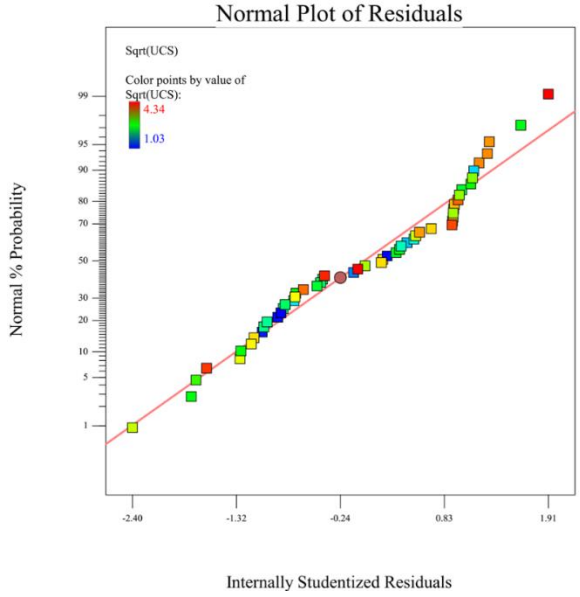

Fig. 13 Normal probability plot for UCS

adopted to estimate the contribution of each parameter and their coupled effect on the response (Montgomery 2001). The statistical properties of the proposed model have been shown in Table 5.

Based on Table 5 the F-value of model indicated it is significant. There is only a 0.01% chance that such a large "Models F-Value" occur due to noise. The "Adequate Precision" measures the signal-to-noise ratio. A ratio greater than 4 is desirable. In addition, the actual and predicted UCS is depicted in Fig. 12 and shows a linear regression relationship.

Response transformation is a crucial component of any data analysis. Transformation is necessary if the error (residuals) is a function of the value of the response. The normality is usually checked by normal plot of the residuals. When there is a pattern in the plot of residuals versus predicted response values, response transformation is

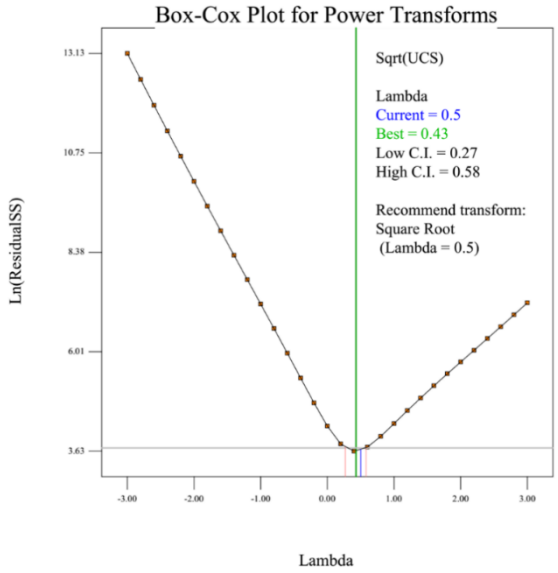

Fig. 14 The Box-Cox plot recommends a power transformation with Lambda=0.5

Table 6 ANOVA of RSM modeling for dependent parameters

Parameters	Sum of Squares	df	Mean Square	F Value	Weighting contribution (%)	P-value
Model	49.32	5	9.86	345.52	16.66	< 0.0001
θ	11.59	1	11.59	406.08	19.58	< 0.0001
2a	35.17	1	35.17	1232.23	59.41	< 0.0001
A	0.15	1	0.15	5.16	0.25	0.0277
θ×2a	1.72	1	1.72	60.11	2.90	< 0.0001
θ^2	0.69	1	0.69	24.04	1.16	< 0.0001
Residual	1.37	48	0.03			
Cor Total	50.69	53				

necessary. Unless the ratio of the maximum response to the minimum response is large, transforming the response will not make much difference (Miller, 1984). The relationship between the normal percentage probability and the studentized residual of model is depicted in Fig. 13.

Therefore, Box-Cox plot (See Fig 14) provides a recommended transformation from the power family as follows:

$$MCS_{Transformed} = (MCS_{Untransformed})^{Lambda},\ Lambda = 0.5 \quad (2)$$

4.4 Multiple regression modeling (MRM)

The best significant MRM was suggested using ANOVA techniques (see Table 6).

Afterwards, by checking model validation, the utility of the model was proved. Th final mathematical model is presented in terms of coded factors (Eq. 3) and actual factors (Eq. 4) as follows:

$$Sqrt\ (UCS) = 2.72 + 0.68 \times \theta\ -\ 0.99 \times 2a - 0.064 \times A + \ 0.32 \times \theta \times 2a\ +\ 0.28 \times \theta^2 \quad (3)$$

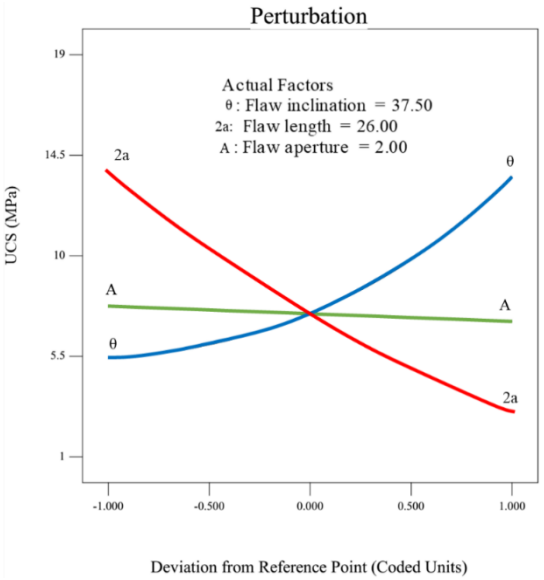

Fig. 15 The effect of flaw inclination, length, and aperture on UCS in terms of coded value

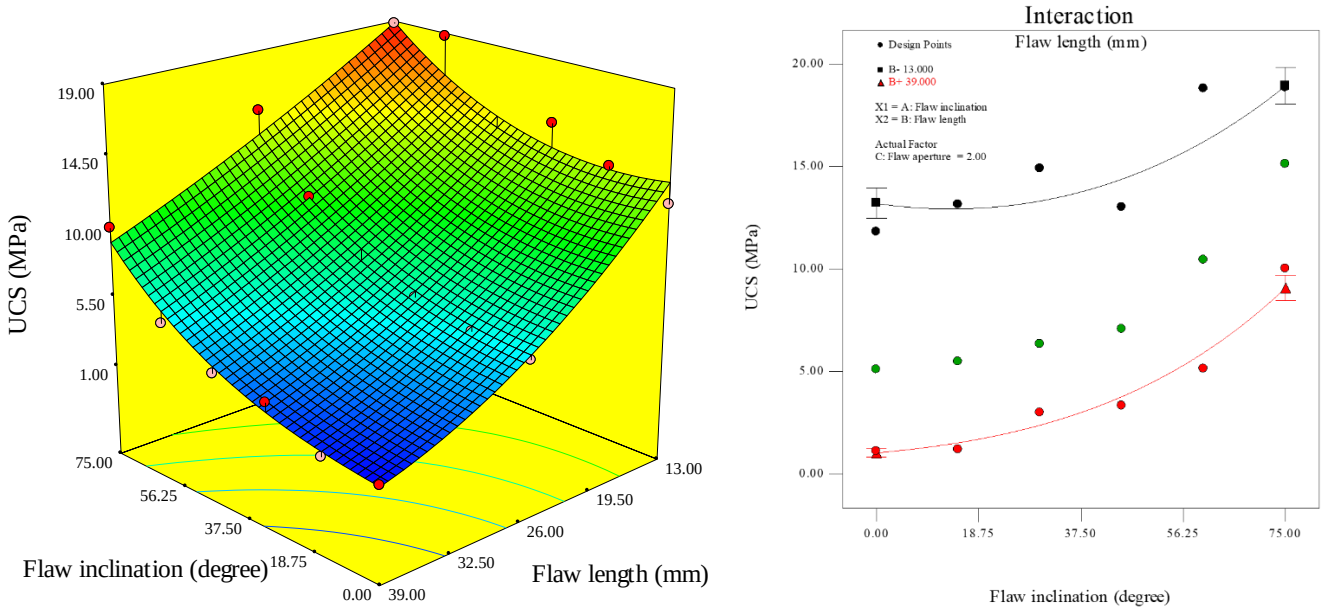

(a) (b)

Fig. 16 Coupled effect of flaw inclination angle and length on the compressive strength of the flawed specimens when another variable is at the middle level (a) Response surface and contour plot and (b) Interaction plot

$$Sqrt\ (UCS) = 5.10098 - 0.014022 \times \theta - 0.10062 \times 2a - 0.079921 \times A + 0.00066 \times \theta \times 2a + 0.0002 \times \theta^2 \quad (4)$$

According to the equations 3 and 4 and Table 6, flaw length has the highest negative effect on specimen strength and flaw angle affect UCS positively secondly. Finally, flaw aperture has the least effect on UCS.

4.5 Analysis of response surface model

The individual effect of flaw parameters as well as their mutual effect on the UCS, have been shown in Figs. 15 and 16. As it can be seen in Fig. 15, when a factor varies, other factors are kept constant at their middle level. The individual effect of θ, 2a and "A" on UCS when other parameters are kept constant is presented in the terms of coded parameters in Fig. 14. According to this plot, by increasing of flaw inclination from 0˚ to 75˚, UCS grows from 5.40 MPa to 13.55 MPa, nonlinearly, and it indicates that increasing of flaw inclination has a positive effect on UCS. Moreover, increasing of flaw length (from 13 mm to 39 mm) leads to UCS reduction from 13.76 MPa to 3.00 MPa. Finally, changes in joint angle from 0° to 75° decreases UCS by 8.90% (From 7.75 MPa to 7.06 MPa), and it indicates that the changes of aperture do not affect the UCS significantly.

Moreover, according to the results of ANOVA, flaw length and inclination mutually affect UCS of specimens, and this interaction effect is shown utilizing surface response and interaction plots in Fig 16. As it can be seen from the plots, when flaw length is constant, by increasing flaw inclination, UCS grows up, whereas when flaw angle is constant, with increasing of flaw length, UCS decreases remarkably. When flaw length is constant at the length of 13 mm, by increasing of flaw inclination from 0˚ to 75˚, UCS increases from 13.19 MPa to 18.93 MPa. When flaw length is 39 mm, with increasing of flaw angle from 0˚ to 75˚, UCS has increased from 1.04 MPa to 9.09 MPa. Furthermore, when flaw inclination is constant at angle of 0˚, by increasing flaw length from 13 mm to 39 mm, UCS decreases from 13.19 MPa to 1.04 MPa. While flaw angle is constant at angle of 75˚, by increasing of flaw length from 13 mm to 39 mm, UCS decreases from 18.95 MPa to 9.09 MPa.

5. Discussion

Many investigations have been conducted on the effect of non-persistent joint parameters the on mechanical response of natural and rock-like specimens (Bahaaddini *et al.* 2013, Huang *et al.* 2016, 2019, Asadizadeh *et al.* 2018a, 2019a, Han *et al.* 2018, Yang *et al.* 2019). Some of them reported that by increasing flaw length UCS decreases (Bahaaddini *et al.* 2013, Han *et al.* 2018, Huang *et al.* 2019, Yang *et al.* 2019), and others indicated that by increasing flaw angle UCS increases, but flaw aperture does not affect UCS (Bahaaddini *et al.* 2013, Asadizadeh *et al.* 2018a, 2019a). Moreover, other researchers studied the effect of non-persistent joints on failure pattern of specimens (Wong and Einstein 2009, Yang *et al.* 2009, Park and Bobet 2010, Yang and Jing 2011, Morgan *et al.* 2013). All of them reported the main three crack types, namely tensile cracks, shear cracks and mixed tensile-shear cracks. The results of this research was classified based on suggestion given by (Wong and Einstein 2009). Therefore, all failure patterns reported in this paper are in high consistency with the output of other research.

As for the UCS trend in filled and unfilled flawed specimens, at $\theta = 75°$ the wing cracks developed at an axial stress level almost near the specimen's UCS, but at low flaw angle they start to initiate at low level of axial stress. This may lead to rapid failure or somehow explosive failure of all specimens with $\theta = 75°$. Moreover, the general trend of unfilled flawed specimens is an increasing trend; however, when the flaw is filled this trend changed to a "U" type anisotropy. The filled flawed specimens are more likely to behave like anisotropic jointed or layered rock mass, and this may happen mainly because of changing the intensity of stress distribution at the tip of cracks and increase bearing capacity of specimen by transferring stress through the filling. Finally, in filled-flawed specimens with $\theta = 75°$, crack development was not as fast as unfilled one, meaning that explosive failure would not happen.

6. Conclusions

A comprehensive experimental study was carried out on the uniaxial compressive strength of synthetic flawed specimens, in which 54 specimens with unfilled flaws were subjected to axial loading and the impact of flaw inclination, length and aperture on UCS was evaluated. In addition, the effect of flaw filling on UCS was investigated, and the results were compared with those of unfilled flaw specimens, and the results were analyzed using AVOVA techniques to investigate the interaction effect of flaw geometry parameters on the UCS. In all flaw geometry, UCS increases by rising flaw inclination, minimum UCS was obtained at the flaw angle of 0˚, and accordingly, the maximum value of UCS occurred at the flaw inclination of 75˚. Additionally, the percentage of UCS reduction at deeper angles of flaw is much more than its reduction at lower angles, and flaw aperture does not contribute to this reduction. Moreover, the peak strength for specimens with filled flaws is more than the peak strength of specimens with unfilled flaw, and for both of them it accrues at high level of flaw inclination. Furthermore, flaw filling changes strength behavior of specimen with increasing flaw inclination from an increasing trend to a typical “U” type anisotropy. Finally, the results of ANOVA revealed the flaw length and inclination mutually affect UCS of flawed specimens, and effect of flaw length on UCS is much more than its inclination while flaw aperture does not affect UCS significantly. However, investigating the effect of strength and deformability of filling material on UCS of flawed specimens would push the frontiers in this field of study.

Conflict of interest

No potential conflict of interest was reported by the authors.

References

Asadizadeh, M. and Rezaei, M. (2019), “Surveying the mechanical response of non-persistent jointed slabs subjected to compressive axial loading utilising GEP approach”, *Int. J. Geotech. Eng*. https://doi.org/10.1080/19386362.2019.1596610.

Asadizadeh, M., Hossaini, M. F., Moosavi, M. and Mohammadi, S. (2016), “A laboratory study on mix design to properly resemble a jointed brittle rock”, *Int. J. Min. Geo-Eng.*, **50**(2), 201-210. https://doi.org/10.22059/ijmge.2016.59830.

Asadizadeh, M., Hossaini, M.F., Moosavi, M., Masoumi, H. and Ranjith, P.G. (2019a), “Mechanical characterisation of jointed rock-like material with non-persistent rough joints subjected to uniaxial compression”, *Eng. Geol.*, **260**, 105224. https://doi.org/10.1016/J.ENGGEO.2019.105224.

Asadizadeh, M., Masoumi, H., Roshan, H. and Hedayat, A. (2019b), “Coupling Taguchi and response surface methodologies for the efficient characterization of jointed rocks’ mechanical properties”, *Rock Mech. Rock Eng.*, **52**(11), 4807-4819. https://doi.org/10.1007/s00603-019-01853-1.

Asadizadeh, M., Moosavi, M. and Hossaini, M.F. (2018a), “Investigation of mechanical behaviour of non-persistent jointed blocks under uniaxial compression”, *Geomech. Eng.*, **14**(1), 29-42. https://doi.org/10.12989/gae.2018.14.1.029.

Asadizadeh, M., Moosavi, M., Hossaini, M.F. and Masoumi, H. (2018b), “Shear strength and cracking process of non-persistent

jointed rocks: An extensive experimental investigation", *Rock Mech. Rock Eng.*, **51**(2), 415-428. https://doi.org/10.1007/s00603-017-1328-6.

ASTM-D7012-14 (2014) D7012-14 Standard test method for compressive strength and elastic moduli of intact rock core specimens under varying states of stress and temperatures.

Bahaaddini, M., Sharrock, G. and Hebblewhite, B.K. (2013), "Numerical investigation of the effect of joint geometrical parameters on the mechanical properties of a non-persistent jointed rock mass under uniaxial compression", *Comput. Geotech.*, **49**, 206-225. https://doi.org/10.1016/j.compgeo.2012.10.012.

Bieniawski, Z.T. and Hawkes, I. (1978), "Suggested methods for determining tensile strength of rock materials", *Int. J. Rock Mech. Min. Sci.*, **15**(3), 99-103.

Bobet, A. (2000), "The initiation of secondary cracks in compression", *Eng. Fract. Mech.*, **66**(2), 187-219. https://doi.org/10.1016/S0013-7944(00)00009-6.

Bobet, A. and Einstein, H.H. (1998), "Fracture coalescence in rock-type materials under uniaxial and biaxial compression", *Int. J. Rock Mech. Min. Sci.*, **35**(7), 863-888. https://doi.org/10.1016/S0148-9062(98)00005-9.

Brady, B.H.G. and Brown, E.T. (2008), *Rock Mechanics for Underground Mining*, *Tunnelling and Underground Space Technology*, Springer.

Chen, X., Liao, Z. and Peng, X. (2012), "Deformability characteristics of jointed rock masses under uniaxial compression", *Int. J. Min. Sci. Technol.*, **22**(2), 213-221. https://doi.org/10.1016/j.ijmst.2011.08.012.

Gemi, L., Köroğlu, M.A. and Ashour, A. (2018), "Experimental study on compressive behavior and failure analysis of composite concrete confined by glass/epoxy ±55° filament wound pipes", *Compos. Struct.*, **187**, 157-168. https://doi.org/10.1016/j.compstruct.2017.12.049.

Han, G., Jing, H., Jiang, Y., Liu, R., Su, H. and Wu, J. (2018), "The effect of joint dip angle on the mechanical behavior of infilled jointed rock masses under uniaxial and biaxial compressions", *Processes*, **6**(5), 49. https://doi.org/10.3390/pr6050049.

Heidarzadeh, S., Saeidi, A. and Rouleau, A. (2018), "Assessing the effect of open stope geometry on rock mass brittle damage using a response surface methodology", *Int. J. Rock Mech. Min. Sci.*, **106**, 60-73. http://doi.org/10.1016/j.ijrmms.2018.03.015.

Huang, C., Yang, W., Duan, K., Fang, L., Wang, L. and Bo, C. (2019), "Mechanical behaviors of the brittle rock-like specimens with multi-non-persistent joints under uniaxial compression", *Constr. Build. Mater.*, **220**, 426-443. https://doi.org/10.1016/j.conbuildmat.2019.05.159.

Huang, Y.H., Yang, S.Q., Tian, W.L., Zeng, W. and Yu, L.Y. (2016), "An experimental study on fracture mechanical behavior of rock-like materials containing two unparallel fissures under uniaxial compression", *Acta Mechanica Sinica*, **3**2(3), 442-455. https://doi.org/10.1007/s10409-015-0489-3.

Kirmizakis, P., Tsamoutsoglou, C., Kayan, B. and Kalderis, D. (2014), "Subcritical water treatment of landfill leachate: Application of response surface methodology", *J. Environ. Manage.*, **146**, 9-15. https://doi.org/10.1016/j.jenvman.2014.04.037.

Lee, H. and Jeon, S. (2011), "An experimental and numerical study of fracture coalescence in pre-cracked specimens under uniaxial compression", *Int. J. Solids Struct.*, **48**(6), 979-999. https://doi.org/10.1016/j.ijsolstr.2010.12.001.

Li, D., Masoumi, H., Saydam, S., Hagan, P.C. and Asadizadeh, M. (2018), "Parametric study of fully grouted cable bolts subjected to axial loading", *Can. Geotech. J.*, **56**(10), 1514-1525. https://doi.org/10.1139/cgj-2018-0470.

Li, Y.P., Chen, L.Z. and Wang, Y.H. (2005), "Experimental research on pre-cracked marble under compression", *Int. J. Solids Struct.*, **42**(9-10), 2505-2516. https://doi.org/10.1016/j.ijsolstr.2004.09.033.

Liu, Q., Xu, J., Liu, X., Jiang, J. and Liu, B. (2015), "The role of flaws on crack growth in rock-like material assessed by AE technique", *Int. J. Fracture*, **193**(2), 99-115. https://doi.org/10.1007/s10704-015-0021-6.

Miller, D.M. (1984), "Reducing transformation bias in curve fittin", *Amer. Stat.*, **38**(2), 124-126. https://doi.org/10.1080/00031305.1984.10483180.

Montgomery, D.C. (2001), *Design and Analysis of Experiments*, John Wiley & Sons, New York, U.S.A., 64-65.

Morgan, S.P., Johnson, C.A. and Einstein, H.H. (2013), "Cracking processes in Barre granite: Fracture process zones and crack coalescence", *Int. J. Fracture*, **180**(2), 177-204. https://doi.org/10.1007/s10704-013-9810-y.

Nemat-Nasser, S. and Horii, H. (1982), "Compression-induced nonplanar crack extension with application to splitting, exfoliation, and rockburst", *J. Geophys. Res.*, **87**(B8), 6805. https://doi.org/10.1029/JB087iB08p06805.

Özbek, Ö. (2021), "Axial and lateral buckling analysis of kevlar/epoxy fiber-reinforced composite laminates incorporating silica nanoparticles", *Polym. Composites*, **42**(3), 1109-1122. https://doi.org/10.1002/pc.25886.

Özbek, Ö. and Bozkurt, Ö. Y. (2019), "Hoop tensile and compression behavior of glass-carbon intraply hybrid fiber reinforced filament wound composite pipes", *Mater. Test.*, **61**(8), 763-769. https://doi.org/10.3139/120.111395.

Özbek, Ö., Bozkurt, Ö.Y. and Erkliğ, A. (2019), "An experimental study on intraply fiber hybridization of filament wound composite pipes subjected to quasi-static compression loading", *Polym. Test.*, **79**, 106082. https://doi.org/10.1016/j.polymertesting.2019.106082.

Özbek, Ö., Doğan, N.F. and Bozkurt, Ö.Y. (2020), "An experimental investigation on lateral crushing response of glass/carbon intraply hybrid filament wound composite pipes", *J. Brazil. Soc. Mech. Sci. Eng.*, **42**(7), 1-13. https://doi.org/10.1007/s40430-020-02475-3.

Özkılıç, Y. O., Yazman, Ş., Aksoylu, C., Arslan, M.H. and Gemi, L. (2021), "Numerical investigation of the parameters influencing the behavior of dapped end prefabricated concrete purlins with and without CFRP strengthening", *Constr. Build. Mater.*, **275**, 122173. https://doi.org/10.1016/j.conbuildmat.2020.122173.

Park, C. H. and Bobet, A. (2010), "Crack initiation, propagation and coalescence from frictional flaws in uniaxial compression", *Eng. Fract. Mech.*, **77**(14), 2727-2748. https://doi.org/10.1016/j.engfracmech.2010.06.027.

Park, C.H. and Bobet, A. (2009), "Crack coalescence in specimens with open and closed flaws: A comparison", *Int. J. Rock Mech. Min. Sci.*, **46**(5), 819-829. https://doi.org/10.1016/j.ijrmms.2009.02.006.

Sagong, M. and Bobet, A. (2002), "Coalescence of multiple flaws in a rock-model material in uniaxial compression", *Int. J. Rock Mech. Min. Sci.*, **39**(2), 229-241. https://doi.org/10.1016/S1365-1609(02)00027-8.

Sodeifian, G., Azizi, J. and Ghoreishi, S. M. (2014) 'Response surface optimization of Smyrnium cordifolium Boiss (SCB) oil extraction via supercritical carbon dioxide', *The Journal of Supercritical Fluids*, 95, pp. 1–7.

Wong, L.N.Y. and Einstein, H.H. (2009), "Systematic evaluation of cracking behavior in specimens containing single flaws under uniaxial compression", *Int. J. Rock Mech. Min. Sci.*, **46**(2), 239-249. https://doi.org/10.1016/j.ijrmms.2008.03.006.

Wong, R.H. and Chau, K.T. (1998), "Crack coalescence in a rock-like material containing two cracks", *Int. J. Rock Mech. Min. Sci.*, **35**(2), 147-164.

https://doi.org/10.1016/S0148-9062(97)00303-3.
Yang, S.Q. and Jing, H.W. (2011), "Strength failure and crack coalescence behavior of brittle sandstone samples containing a single fissure under uniaxial compression", *Int. J. Fracture*, **168**(2), 227-250. https://doi.org/10.1007/s10704-010-9576-4.
Yang, S.Q., Dai, Y.H., Han, L.J. and Jin, Z.Q. (2009), "Experimental study on mechanical behavior of brittle marble samples containing different flaws under uniaxial compression", *Eng. Fract. Mech.*, **76**(12), 1833-1845. https://doi.org/10.1016/j.engfracmech.2009.04.005.
Yang, S.Q., Jiang, Y.Z., Xu, W.Y. and Chen, X.Q. (2008), "Experimental investigation on strength and failure behavior of pre-cracked marble under conventional triaxial compression", *Int. J. Solids Struct.*, **45**(17), 4796-4819. https://doi.org/10.1016/j.ijsolstr.2008.04.023.
Yang, W., Li, G., Ranjith, P.G. and Fang, L. (2019), "An experimental study of mechanical behavior of brittle rock-like specimens with multi-non-persistent joints under uniaxial compression and damage analysis", *Int. J. Damage Mech.*, **28**(10), 1490-1522. https://doi.org/10.1177/1056789519832651.
Yin, Q., Jing, H. and Su, H. (2018), "Investigation on mechanical behavior and crack coalescence of sandstone specimens containing fissure-hole combined flaws under uniaxial compression", *Geosci. J.*, 1-18.
Yuan, Z., Yang, J., Zhang, Y. and Zhang, X. (2015), "The optimization of air-breathing micro direct methanol fuel cell using response surface method", *Energy*, **80**, 340-349. https://doi.org/10.1016/j.energy.2014.11.076.

CC